Nonlinear waves in networks: Model reduction for the sine-Gordon equation

Jean-Guy Caputo[*]
Laboratoire de Mathématiques, INSA de Rouen, 76801 Saint-Etienne du Rouvray, France

Denys Dutykh[†]
LAMA, UMR 5127 CNRS, Université de Savoie, Campus Scientifique, 73376 Le Bourget-du-Lac Cedex, France
(Received 26 February 2014; revised manuscript received 18 June 2014; published 25 August 2014)

To study how nonlinear waves propagate across Y- and T-type junctions, we consider the two-dimensional (2D) sine-Gordon equation as a model and examine the crossing of kinks and breathers. Comparing energies for different geometries reveals that, for small widths, the angle of the fork plays no role. Motivated by this, we introduce a one-dimensional effective model whose solutions agree well with the 2D simulations for kink and breather solutions. These exhibit two different behaviors: a kink crosses if it has sufficient energy; conversely a breather crosses when $v > 1 - \omega$, where v and ω are, respectively, its velocity and frequency. This methodology can be generalized to more complex nonlinear wave models.

DOI: 10.1103/PhysRevE.90.022912 PACS number(s): 05.45.Yv, 74.81.Fa

I. INTRODUCTION

The propagation of nonlinear waves in networks is a very common problem. Examples are the nerve impulse traveling in arrays of neurons [1], the motion of the pulse wave in the arterial circulatory system [2], or the propagation of waves in the electrical power grid [3]. In general the problem is difficult to tackle because both the equation of motion and the geometry are complex. A first direction is to consider a simpler geometry like a Y junction (see Fig. 1). Another simplification is to study what happens for a linear wave equation. In this context, a number of researchers have examined so-called quantum graphs where the Schrödinger equation is solved on a network. See Ref. [4] for a review. For these linear systems, the scattering formalism can be employed and this gives the reflection and transmission coefficients for a harmonic wave. This is detailed specifically for a Y junction and for the Klein-Gordon linear wave equation in Ref. [5].

In many cases however, the nonlinearity cannot be neglected. For fluid systems, note the works by Bona and Cascaval [6] and Mugnolo and Rault [7] who used the Benjamin-Bona-Mahoney (BBM) shallow water equation to describe a fluid network. The authors used the fact that the BBM equation is unidirectional; hence, most of the energy is propagated downstream. For the Boussinesq equation in a junction, Nachbin and Da Silva Simoes [8] used a conformal map technique. However, all these studies do not provide a simple understanding of the behavior of the waves; in particular, one cannot see easily how energy travels across the network.

To address these issues, a first step is to consider a simpler model. For instance, before tackling the propagation of shallow water waves in a river basin, for which there are two variables, the water elevation and the potential flow, it is useful to consider a simpler nonlinear hyperbolic equation. The sine-Gordon equation is precisely a simple nonlinear hyperbolic equation that admits localized solutions. It is also a Hamiltonian system in any dimension, integrable in one dimension so that one can compare the numerical solutions with their exact counterpart as they propagate in a one-dimensional (1D) channel. Finally, the sine-Gordon equation is an excellent model of an extended Josephson junction between two superconductors [9]. Here, to simplify the issue and to keep the Hamiltonian framework, we exclude external actions on the network, like a current or a magnetic field, that are commonly used in Josephson junction arrays.

Consider the two-dimensional (2D) sine-Gordon equation defined in a Y junction such as that shown in Fig. 1. A first work on the problem is by Gulevich and Kusmartsev [10] who examined numerically how kinks propagate in such a system, in the context of Josephson junctions. They showed that the kink needs a sufficient velocity to cross the branch. Here we follow up on this and define a 2D symmetric junction parametrized by the angle θ between the branches and by the widths w_1 and w_2 of the branches. This setup can describe a Y junction up to a T junction ($\theta = 180^\circ$). We solve the 2D problem using the `FreeFem++` finite element library [11]. It is important that the energy is conserved by the code; for this we found a suitable time discretization. The study of the propagation of a kink in the junction yielded the immediate result that for small widths there is no dependence of the velocity on the angle of the fork for the full 2D simulation. We therefore introduce a 1D effective partial differential equation to capture the essential features of the 2D propagation. This model incorporates the junction, using the ideas of graph Laplacian [12]; its solutions agree well with the 2D solutions. For the kink propagation in a junction we confirm the existence of a critical velocity given approximately by the simple energy conservation argument. Below this velocity, the kink gets reflected by the fork. Above it, it passes through the junction and splits into two kinks that propagate in the two different branches. For breathers there are two parameters, ω the frequency and v the velocity. For a given velocity v, junction crossing is only possible above the frequency $\omega \approx 1 - v$, indicating a nonlinear resonance. After the breather passes through the junction it gives rise to new breathers in the

[*]caputo@insa-rouen.fr; https://sites.google.com/site/jeanguycaputo
[†]Denys.Dutykh@univ-savoie.fr; http://www.denys-dutykh.com/

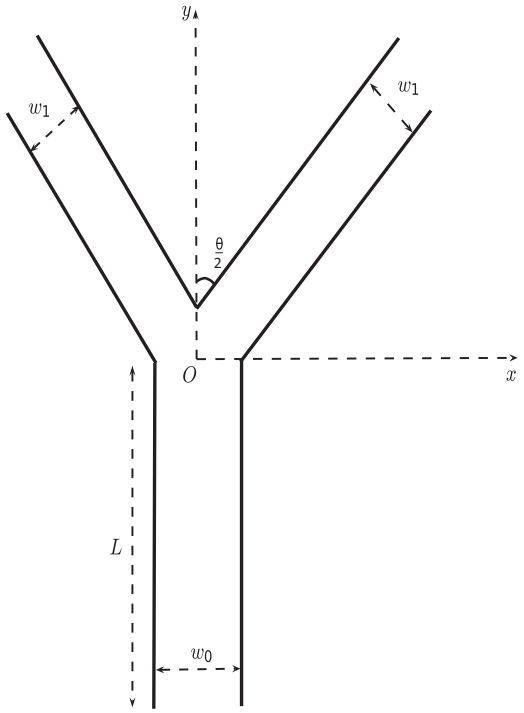

FIG. 1. Sketch of the computational domain Ω.

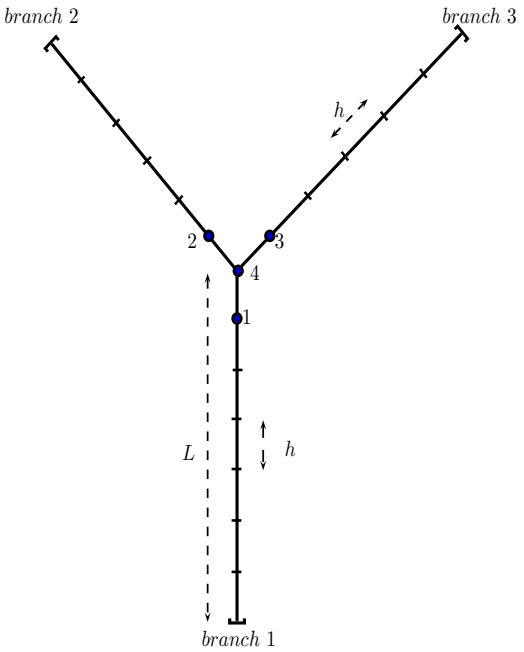

FIG. 2. (Color online) Sketch of the tree geometry for the 1D effective model.

branches. We characterize these using their energy density and estimate their velocity and frequency. We always observe an upshift of the frequency and a slight downshift of the velocity.

The article is organized as follows. In Sec. II we derive the 1D effective model from the 2D sine-Gordon equation defined in the fork. In Sec. III we recall the energies for the kink and the breather and show how they can be used to estimate a critical velocity. Section IV introduces energy conserving discretizations for the finite element 2D problem and the 1D effective equation. Their solutions are compared in Sec. V for both kink and breather initial conditions. Conclusions are presented in Sec. VI.

II. THE 1D EFFECTIVE SINE-GORDON MODEL

We consider the 2D sine-Gordon equation

$$\varphi_{tt} - \Delta\varphi + \sin\varphi = 0, \tag{1}$$

on a bounded domain $\Omega \subset \mathbb{R}^2$ with Neuman boundary conditions,

$$\nabla\varphi \cdot \mathbf{n} = 0,$$

where $\mathbf{n}$ is an exterior normal. The t subscript indicates the time derivative and Δ is the usual Laplacian in spatial coordinates. This equation conserves the energy:

$$\mathcal{E} = \int_\Omega \left[\frac{1}{2}\varphi_t^2 + \frac{1}{2}|\nabla\varphi|^2 + (1-\cos\varphi)\right] dx\,dy. \tag{2}$$

This can be checked easily by multiplying Eq. (1) by φ_t, integrating over the domain, and using the Stokes formula for the spatial operator.

Since the boundary conditions of the 2D problem are homogeneous Neuman it is natural to assume that the solution is uniform in the transverse direction. In other words we keep only the first transverse Fourier mode. Then Eq. (1) reduces in each branch to a 1D sine-Gordon equation,

$$\varphi^i_{tt} - \varphi^i_{xx} + \sin\varphi^i = 0, \quad i = 1,2,3, \tag{3}$$

where the label i corresponds to the three branches as shown in Fig. 2. These equations are coupled at the apex by two conditions; one is the continuity of φ^i,

$$\varphi^1(x=l) = \varphi^2(x=0) = \varphi^3(x=0)\,, \tag{4}$$

and the other is the flux conservation or the Kirchoff law,

$$-w_1\varphi^1_x + w_2\varphi^2_x + w_3\varphi^3_x = 0, \tag{5}$$

where φ^i_x is the normal velocity in branch i. Let us now briefly justify this flux relation. For that, consider the fork domain F obtained by taking the normals at the different branches as close as possible to the fork as shown in Fig. 3. Integrating the 2D equation, Eq. (1), on F yields

$$\int_F (\varphi_{tt} + \sin\varphi)dxdy - \int_{\partial F} \nabla\varphi \cdot \mathbf{n} ds = 0, \tag{6}$$

where $\mathbf{n}$ is the normal to the edge of the domain ∂F. The second term is equal to the left-hand side of Eq. (5). The first one is of order w^2, where w is the typical width of the branches. In the limit of small w, such that $w_i \to 0$ with w_2/w_1 and w_2/w_1 constant, the first term vanishes while the second one remains, yielding Eq. (5)

The numerical scheme used to solve this 1D effective model is described below (see Sec. IV); it is a finite difference approximation. The junction corresponds to the four nodes highlighted in Fig. 2; these are labeled as 1, 2, and 3 for the three branches and are connected to the central node 4. The outer nodes are the last nodes updated by the partial differential equation solver; let us name the value of the solution there φ_1,

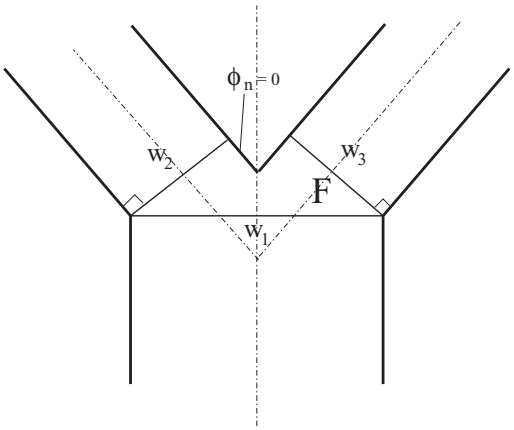

FIG. 3. The fork region F.

φ_2, and φ_3 for each branch. The value at the central node φ_4 can be computed from the interface conditions (4) and (5). Using a forward finite difference approximation for φ_x^i we get the following from Eq. (5):

$$-w_1(\varphi_4-\varphi_1)+w_2(\varphi_2-\varphi_4)+w_3(\varphi_3-\varphi_4)=0,$$

where we have assumed the same space step on the three branches and used the notation $\varphi_i \equiv \varphi(x_i)$. We have also omitted the j index corresponding to the different branches. We then obtain

$$\varphi_4=\frac{w_1\varphi_1+w_2\varphi_2+w_3\varphi_3}{w_1+w_2+w_3}. \tag{7}$$

III. THEORETICAL CONSIDERATIONS

In 1D the sine-Gordon equation is integrable (see, for example, Ref. [1]). It has two families of localized exact solutions, the kink,

$$\varphi(x,t)=4\arctan\{\exp[\gamma(x-vt)]\}, \tag{8}$$

and the breather [13],

$$\varphi(x,t)=4\arctan\left[\frac{\sqrt{1-\omega^2}\cos[\omega\gamma(t-vx)]}{\omega\cosh[\sqrt{1-\omega^2}\gamma(x-vt)]}\right], \tag{9}$$

where the Lorentz factor γ is given by

$$\gamma=\frac{1}{\sqrt{1-v^2}}. \tag{10}$$

Let us first consider the kink, its energy is

$$\mathcal{E}_k=8\gamma. \tag{11}$$

The energy of the breather depends also on the frequency, it is given by

$$\mathcal{E}_b=16\gamma\sqrt{1-\omega^2}. \tag{12}$$

In two dimensions the equation is not integrable. In addition there is the complication of the boundaries. Therefore the only relations that can be used are conservation laws, and in particular the conservation of energy. When the kink is in branch 1, its energy is $8w_1\gamma$ because it is homogeneous in the transverse direction. Similarly in branch 2, it has energy $8w_2\gamma_2$. The conservation of energy reads

$$w_1\frac{8}{\sqrt{1-v_1^2}}=2w_2\frac{8}{\sqrt{1-v_2^2}}, \tag{13}$$

where we assume $w_2=w_3$. This expression gives a critical velocity v_1 for which $v_2=0$:

$$v_k=\sqrt{1-\left(\frac{w_1}{2w_2}\right)^2}. \tag{14}$$

This formula was derived in Ref. [10] and compared successfully to the 2D numerical results for a fixed angle and widths $w_3=w_1$, $0<w_2/w_1<1$. In the next section we confirm this estimate by numerical simulations and show its limitations.

A similar argument for the breather yields the following result for the parameters $\{v_1,\omega_1\}$ in the bottom branch and the parameters $\{v_2,\omega_2\}$ in the top branches:

$$\frac{v_1^2-1}{\omega_1^2-1}=\left(\frac{w_1}{2w_2}\right)^2\frac{v_2^2-1}{\omega_2^2-1}. \tag{15}$$

This gives a critical velocity v_1 for which $v_2=0$:

$$v_k=\sqrt{1-\frac{\omega_1^2-1}{\omega_2^2-1}\left(\frac{w_1}{2w_2}\right)^2}. \tag{16}$$

The practical application of the previous formula is difficult because ω_2 remains unknown. Note however that for small amplitudes, i.e., in the linear limit, $\omega_1=\omega_2$ so that we recover Eq. (14) for the critical velocity.

IV. NUMERICAL METHODS

We now describe the numerical methods used to solve the 2D and the 1D effective problems. Equation (1) is solved using the finite element method. For that recall the standard scalar product in $L^2(\Omega)$:

$$(\varphi,\psi)\equiv\int_\Omega\varphi\psi\,dxdy.$$

Using this scalar product we project the operator on a test function and use the Green's theorem to integrate the Laplacian [14]. The second derivative in time is approximated by the standard three-step discretization. We also average the Laplacian over the current and the following time steps. The final semidiscrete scheme is the following weak formulation:

$$\frac{1}{\Delta t^2}(\varphi^{n+1}-2\varphi^n+\varphi^{n-1},\psi)+\frac{1}{2}[\nabla(\varphi^{n+1}+\varphi^n),\nabla\psi]+(\sin\varphi^n,\psi)=0, \tag{17}$$

where $\psi\in L_2(\Omega)$ is the test function; Δt is the time step; and φ^{n-1}, φ^n, and φ^{n+1} are, respectively, the solution at times steps t_{n-1}, t_n, and t_{n+1}, where $t_j=j\Delta t$. For the spatial discretization we use a nonstructured triangular mesh with $\mathbb{P}_2$ finite element space. The computations are performed using the `FreeFem++` open-source software [11]. The boundary conditions are set to be homogeneous Neuman:

$$\nabla\varphi\cdot\mathbf{n}=0,$$

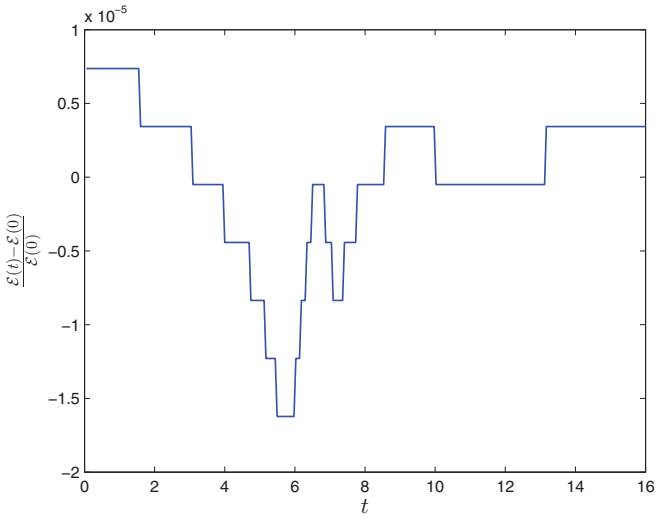

FIG. 4. (Color online) Relative energy $|\mathcal{E}_n - \langle\mathcal{E}_n\rangle|/\langle\mathcal{E}_n\rangle$ as a function of time for the 2D finite element solution of a breather propagating in a 2D domain.

where **n** is the exterior normal to the boundary of the domain Ω.

The total discrete energy is calculated as

$$\mathcal{E}_n = \frac{1}{2}\int\left[\left(\frac{\varphi^{n+1}-\varphi^{n-1}}{2\Delta t}\right)^2 + |\nabla\varphi^n|^2 - 2(1-\cos\varphi^n)\right]dxdy. \qquad (18)$$

This quantity is conserved up to order $O(h^4)$, where h is the typical space step. There is no trend in the relative error on the total energy $|\mathcal{E}_n - \mathcal{E}_0|/\mathcal{E}_0$ in the course of the computations as shown in Fig. 4. This plot corresponds to the breather of velocity $v = 0.8$ and frequency $\omega = 0.3$ crossing the fork (see Sec. V). For a kink the error is even smaller. In the numerical simulations presented below, we used the mesh with a typical size $\Delta x \approx 0.05$ and the time step $\Delta t = 0.0075$. Because of the implicit nature of Eq. (17), we could take a much bigger time step. However, we preferred to keep it small enough in order to reduce the time discretization error.

The 1D effective problem is solved using the finite difference method. The scheme employed reads

$$\frac{\varphi_j^{n+1}+\varphi_j^{n-1}-2\varphi_j^n}{\Delta t^2} - \frac{\varphi_{j+1}^n+\varphi_{j-1}^n-2\varphi_j^n}{\Delta x^2} + \sin\varphi_j^n = 0, \qquad (19)$$

where n and j are, respectively, the time and space indices. Despite the simplicity of Eq. (19) it can be shown that it is a symplectic Euler method derived for the sine-Gordon equation recast in Hamiltonian form [15]. Consequently, the 1D scheme is stable and conserves energy. Typical values of the space step and the time step are $\Delta x = 0.05$ and $\Delta t = 0.01$.

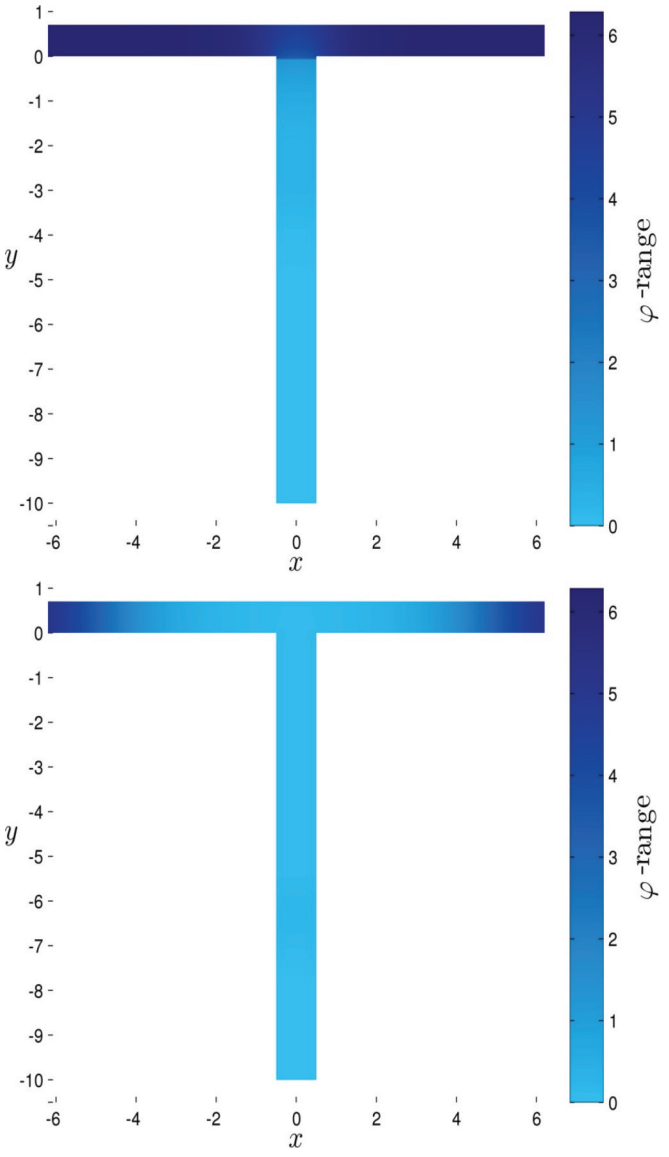

FIG. 5. (Color online) Motion in a T junction. Snapshots of a kink starting in branch 1 with the velocity $v_1 = 0.75$. The times are $t = 1350$ (top) and $t = 3000$ (bottom).

V. NUMERICAL RESULTS

We first consider the propagation of a kink in the Y and T junctions. As expected the kink gets reflected if it does not have enough energy (velocity). Also the motion depends very weakly on the angle. To illustrate this fact, we show in Fig. 5 a kink propagating in a T junction and crossing it. We take the same kink and run it into a Y junction. This is shown in Fig. 6. One can see that the time intervals for propagation are about the same. This is confirmed by examining the evolution of the energy in the branches 1 (bottom) and 2 (left) (see Fig. 7). Note also that a very small amount of energy, typically 5% of the total energy, is left in branch 1 once the kink has crossed over into branches 2 and 3. The solution of the 1D effective model is plotted with points in Fig. 7; it agrees very well with the 2D solution and this confirms the informal asymptotic reduction from 2D to 1D of the previous section.

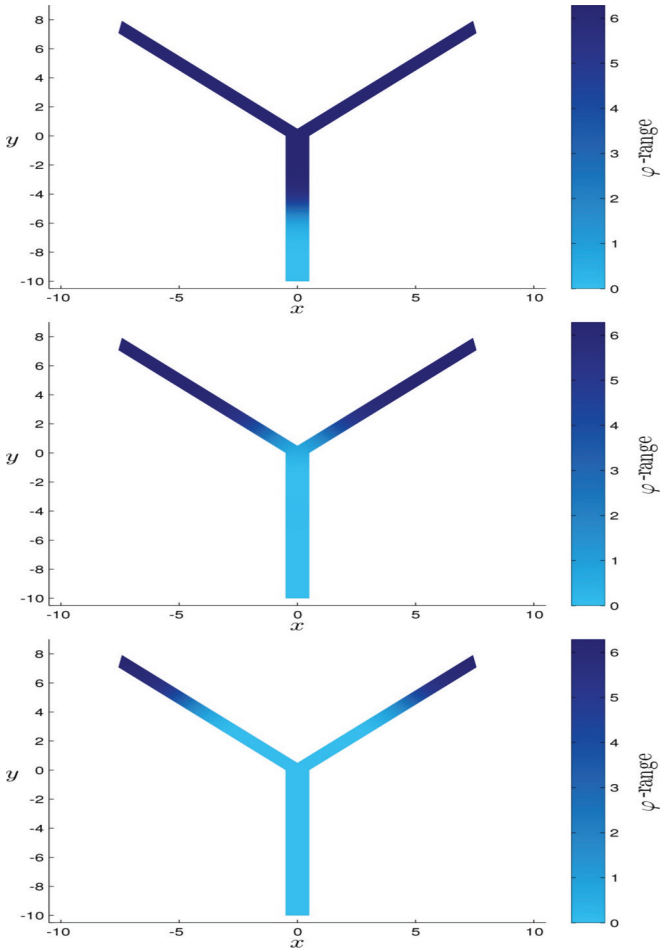

FIG. 6. (Color online) Motion of a kink in a 90° Y junction. Snapshots of a kink starting in branch 1 with the velocity $v_1 = 0.75$. The times are $t = 900$ (top), $t = 1500$ (middle), and $t = 3500$ (bottom). The widths are $w_1 = 1$ and $w_2 = w_3 = 0.7$.

We now compare systematically the 2D solution with that of the 1D effective equation. To validate this approximation, we conduct a parametric study choosing w_1, w_2, and w_3 such that $w_1 = 1$ and $w_2 = w_3 = w_1 + \alpha$, where $\alpha = -0.3, -0.1$, 0.1, and 0.3. The results for the critical velocity as well as the estimate (14) are reported in the Table I. The 2D and 1D models are very close even for $\alpha > 0$. On the other hand the energy estimate is a lower estimate for $\alpha > 0$. The 2D and 1D effective results reveal that the kink crosses the junction but that there are oscillations. The front seems to oscillate and then reshape as it enters more into branches 2 and 3. We do not see this effect when $\alpha \leqslant 0$. Despite this, the values are all within a 10% interval of error. To check the 2D-1D reduction even further, we conducted simulations with the large width $w_1 = w_2 = w_3 = 10$ for large and small velocities. We found that for the small velocity $v_1 = 0.75$ the kink gets reflected and significant transverse oscillations occur. These transverse oscillations are the ones that propagate along the equal phase contour lines; they were studied by Gulevitch *et al.* [16] who showed that their dispersion is $\omega = k$. In this situation, the angle becomes important and of course the 2D and the 1D models disagree. On the other hand, for the large velocity $v_1 = 0.96$, the kink crosses and the transverse oscillations remain small. Then the 2D and the 1D models are very close.

TABLE I. Kink critical velocities for the 2D model, the 1D effective model, and the energy estimate as a function of α. The widths of the branches are $w_1 = 1$ and $w_2 = w_3 = w_1 + \alpha$.

α	2D v_c	1D v_c	v_k From Eq. (14)
0.3	0.98	0.99	0.92
0.1	0.965	0.955	0.89
0	0.92	0.94	0.86
−0.1	0.885	0.85	0.83
−0.3	0.73	0.71	0.7

For the breather, things are more complicated because of the additional parameter, the frequency. The energy criterion is not sufficient, the breather needs to have the adapted frequency in order to cross. To illustrate this, we consider a breather of initial velocity $v_1 = 0.4$ and different frequencies. Figure 8 shows the energy E_1 in branch 1 as a function of time for frequencies $\omega_1 = 0.5, 0.7, 0.725$, and 0.75. The breather does

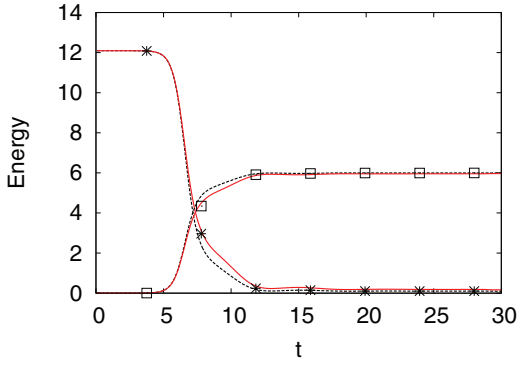

FIG. 7. (Color online) Time evolution of the energy for the kink motion in branches 1 and 2 for the T junction, shown as the solid line (red online), and for the Y junction, shown as the dashed line. The energy for the 1D effective model is plotted with points. The parameters are the same as those in Figs. 5 and 6.

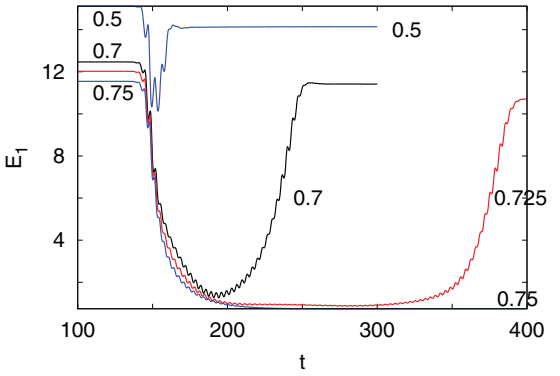

FIG. 8. (Color online) Energy in branch 1 as a function of time for the 1D model and a breather of initial velocity $v_1 = 0.4$ and frequencies $\omega_1 = 0.5, 0.7, 0.725$, and 0.75. Notice the crossing for $\omega_1 = 0.75$. The widths are $w_1 = w_2 = w_3 = 1$.

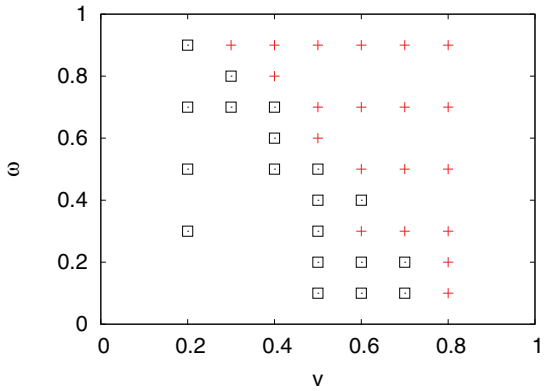

FIG. 9. (Color online) Parameter space (v,ω) for the crossing of breathers for the 2D and the 1D models. The crosses (red online) indicate crossing and the squares reflection. The widths are $w_1 = w_2 = w_3 = 1$.

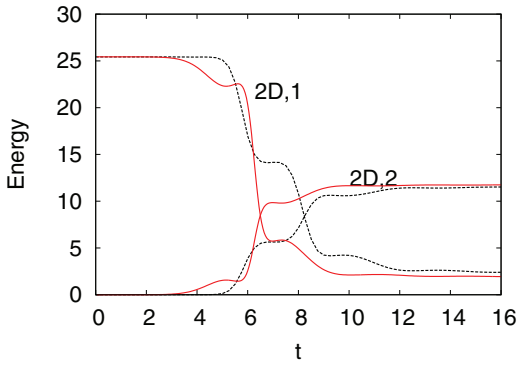

FIG. 10. (Color online) Time evolution of the energy in branches 1 and 2 for a breather for the 2D partial differential equation, shown as the solid line (red online), and the 1D effective model, shown as the dashed line. The parameters are $w_1 = w_2 = w_3 = 1$, $v_1 = 0.8$, $\omega_1 = 0.3$, and $x_0 = 10$.

not cross until the frequency reaches 0.75; for this frequency the initial energy is smaller than for $\omega_1 = 0.5$. The initial energy will not determine crossing, the initial frequency will. Another interesting effect is that for $\omega_1 = 0.725$ the energy E_1 almost goes to 0 in the time interval $[200; 300]$—as if the breather crossed the junction—and then it returns almost to its initial value, indicating reflection. We checked the position of the breather and found that it stays with an interval of size 10 close to the junction. This long oscillation close to the junction could indicate a nonlinear bound state associated with the fork.

Figure 9 shows the crossing vs noncrossing in the parameter space (v,ω). The crossing (reflection) of the breather is indicated by the $+$ $(\times)$ sign. The calculations were done both with the 1D effective model and with the full 2D equations and the results always agreed. For sufficiently large velocities, the breather crosses independently of its frequency. On the other hand, for frequencies close to one, the breather crosses even for small velocities. This situation is close to the linear case for which we expect always some energy transfer to the other branch [5]. There is always a small reflection from the fork. For example, we show the time evolution of the energy of a breather in Fig. 10. Notice how the energy in branch 1 does not drop to zero like for the kink. There is a remainder. The small scale oscillations present in Fig. 10 are the ones seen in Fig. 8; at this time we do not know their origin.

To characterize the breathers in the other branches is difficult because the wave oscillates. We found that plotting the energy density,

$$d\mathcal{E} = \tfrac{1}{2}\varphi_t^2 + \tfrac{1}{2}\varphi_x^2 + 1 - \cos\varphi, \qquad (20)$$

gives a good indication of the position of the breather. Let us analyze in more detail the specific configuration where a breather of speed $v = 0.8$ and frequency $\omega = 0.3$ crosses the junction. Figure 11shows the energy density for three different times in branch 1 (top panel) and in branch 2 (bottom panel) after the breather has passed the junction. Then the energies in branch 1 and branch 2 are, respectively, $\mathcal{E}_1 = 2.16$ and $\mathcal{E}_2 = 13.23$. The velocities estimated by a least-square fit on the center of mass of the breather density are, respectively, $v_1 = -0.75$ and $v_2 = 0.6$. They are lower than the initial velocity to accommodate for the crossing of the breather. The frequencies of the breathers in branches 1 and 2 can be estimated; they are, respectively, $\omega_1 = 0.996$ and $\omega_2 = 0.75$. All these parameters are very different from the initial breather parameter, making the scattering of a breather much more complex than the one of a kink.

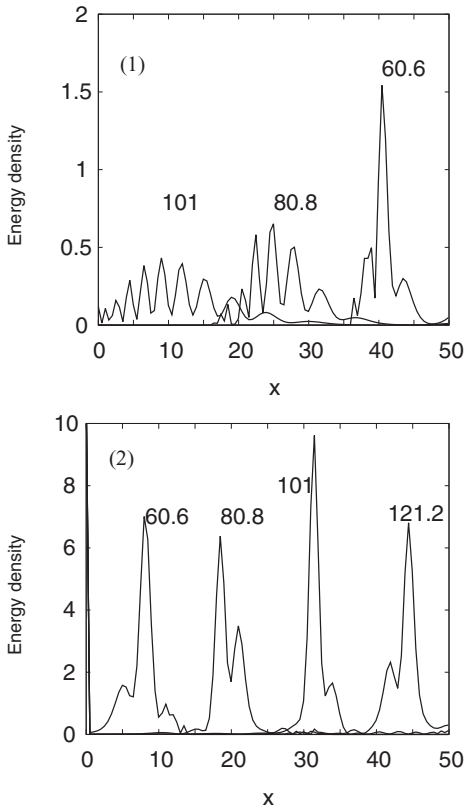

FIG. 11. Snapshots of the energy density of a breather at different times in branches 1 (top) and 2 (bottom). The times are indicated on the plots. The parameters are $w_1 = w_2 = w_3 = 1$, $v_1 = 0.8$, and $\omega_1 = 0.3$. The initial position of the breather is $x_0 = 10$.

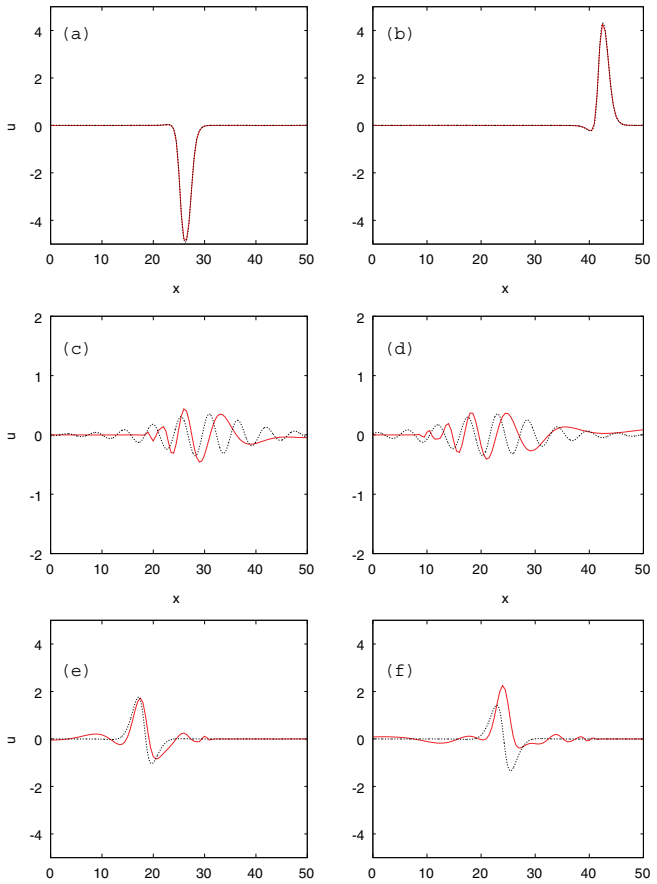

FIG. 12. (Color online) Snapshots of the breather analytical solution (dashed line) together with the numerical solution (continuous line), in branch 1 before the collision [panels (a) and (b)], in branch 1 after the collision [panels (c) and (d)], and in branch 2 [panels (e) and (f)]. The corresponding times are $t = 20.2, 40.4, 80.8, 90.9$ for panels (a)–(d) and $t = 80.8, 90.9$ for panels (e) and (f).

Using the parameters above we can plot the fitted breathers and compare them with the numerical solution. Figure 12 shows, in the top panel, branch 1 before the breather crosses. There the analytical solution matches perfectly the numerical one. The middle and bottom panels show, respectively, branch 1 after the crossing and branch 2. Here the agreement is not as good but remains quite acceptable. The reflected breather in branch 1 (middle panel) has a small amplitude of about 0.2. Its frequency as seen from Table II is 0.99 so that it is very close to the dispersion curve $\omega = \sqrt{1+k^2}$. This can explain the dispersion observed.

To conclude this study we examine systematically the influence of the breather frequency on its crossing. We took $v_1 = 0.8$ and chose $\omega_1 = 0.3, 0.5, 0.7$, and 0.9. The results are reported in Table II.

TABLE II. Velocities and frequencies for the crossing of a breather of initial velocity $v_1 = 0.8$ and different frequencies $\omega_1 = 0.3$ and 0.5 (top rows) and $\omega_1 = 0.7$ and 0.9 (bottom rows). The columns indicate the branches, 1, 1-return and 2. The label "1-return" corresponds to branch 1 after the collision.

Branch index i	1	1-return	2	1	1-return	2
ω_i	0.3	0.99	0.79	0.5	0.99	0.87
v_i	0.8	0.8	0.56	0.8	0.8	0.65
Energy E	25.42	2.1	11.66	23.07	2.12	10.48
ω_i	0.7	0.998	0.93	0.9	0.999	0.98
v_i	0.8	0.85	0.73	0.8	0.85	0.8
Energy E	19.03	1.91	8.57	11.61	1.23	5.192

VI. CONCLUSION

We analyzed numerically and theoretically how a 2D sine-Gordon kink or breather crosses a Y or T junction. Comparing the energies in the different branches for both cases revealed that the angle of the junction plays almost no role in the dynamics for thin trees. This suggested to introduce a 1D effective model where, at the junction, we satisfy continuity of the solution and flux conservation. The solutions of this effective model accurately reproduce the 2D solutions.

The parameters for the kink to cross obey the simple relation obtained from the conservation of energy. There is a critical velocity below which no crossing is possible.

Breather crossing is more complex because there are two parameters: the velocity v and the frequency ω. For equal widths of the branches, we observe crossing when $v > 1 - \omega$. Then the breather gives rise to two other breathers in the two upper branches that we characterize using the energy density and the value of the energy. These new breathers are slower than the initial condition and are also upshifted in frequency. We always observe a small reflection at the crossing into the first branch.

This study can be extended by considering more branches. Another interesting extension would be to add a source at the junction, enabling us to control the crossing. It would be useful to understand how to transpose this to another application, like the reflection of shallow water waves.

ACKNOWLEDGMENTS

D.D. acknowledges the support from ERC under Research Project No. ERC-2011-AdG 290562-MULTIWAVE and thanks INSA de Rouen for its hospitality during his visit in December 2012. The authors thank D. Mitsotakis and G. Sadaka for useful discussions on the finite element numerical method. The authors acknowledge the Centre de Ressources Informatiques de Haute Normandie where most of the calculations were done.

[1] A. C. Scott, *Nonlinear Science, Emergence and Dynamics of Coherent Structures* (Oxford University Press, London, 2003).

[2] *McDonald's Blood Flow in Arteries*, Sixth Edition: Theoretical, Experimental and Clinical Principles, edited by W. Nichols, M. O'Rourke, and C. Vlachopoulos (CRC Press, Boca Raton, FL, 2011).

[3] S. Backhaus and M. Chertkov, Phys. Today **66**, 42 (2013).

[4] S. Gnutzmann and U. Smilansky, Adv. Phys. **55**, 527 (2006).

[5] P. N. Bibikov and L. V. Prokhorov, J. Phys. A: Math. Theor. **42**, 045302 (2009).
[6] J. L. Bona and R. C. Cascaval, Can. App. Math. Q. **16**, 1 (2008).
[7] D. Mugnolo and J. F. Rault, arXiv:1302.2104.
[8] A. Nachbin and V. Da Silva Simões, J. Nonlinear Math. Phys. **19**, 116 (2012).
[9] A. Barone and G. Paterno, *Physics and Applications of the Josephson Effect* (Wiley, New York, 1982).
[10] D. R. Gulevich and F. V. Kusmartsev, Phys. Rev. Lett. **97**, 017004 (2006).
[11] F. Hecht, J. Numer. Math. **20**, 251 (2013).
[12] J.-G. Caputo, A. Knippel, and E. Simo, J. Phys. A: Math. Theor. **46**, 035101 (2013).
[13] R. K. Dodd, J. C. Eilbeck, J. D. Gibbon, and H. C. Morris, *Solitons and Nonlinear Wave Equations* (Academic Press, San Diego, 1984).
[14] J. Argyris, M. Haase, and J. C. Heinrich, Comp. Methods Appl. Mech. Eng. **86**, 1 (1991).
[15] B. Leimkhuler and S. Reich, *Simulating Hamiltonian Dynamics* (Cambridge University Press, Cambridge, UK, 2004).
[16] D. R. Gulevich, S. Savelev, V. A. Yampolskii, F. V. Kusmartsev, and F. Nori, J. Appl. Phys. **104**, 064507 (2008).